# Conserved patterns of functional organization between cortex and thalamus in mice

Andrew J. Miller-Hansen[a] (ID) and S. Murray Sherman[a,1] (ID)

Higher-order thalamic nuclei contribute to sensory processing via projections to primary and higher cerebral cortical areas, but it is unknown which of their cortical and subcortical inputs contribute to their distinct output pathways. We used subpopulation specific viral strategies in mice to anatomically and physiologically dissect pathways of the higher-order thalamic nuclei of the somatosensory and visual systems (the posterior medial nucleus and pulvinar). Employing a complementary optogenetics and electrical stimulation strategy, we show that synapses in cortex from higher-order thalamus have functionally divergent properties in primary vs. higher cortical areas. Higher-order thalamic projections onto excitatory targets in S1 and V1 were weakly modulatory, while projections to S2 and higher visual areas were strong drivers of postsynaptic targets. Then, using transsynaptic tracing verified by optogenetics to map inputs to higher-order thalamus, we show that posterior medial nucleus cells projecting to S1 are driven by neurons in layer 5 of S1, S2, and M1 and that pulvinar cells projecting to V1 are driven by neurons in layer 5 of V1 and higher visual areas. Therefore, in both systems, layer 5 of primary and higher cortical areas drives transthalamic feedback modulation of primary sensory cortex through higher-order thalamus. These results highlight conserved organization that may be shared by other thalamocortical circuitry. They also support the hypothesis that direct corticocortical projections in the brain are paralleled by transthalamic pathways, even in the feedback direction, with feedforward transthalamic pathways acting as drivers, while feedback through thalamus is modulatory.

thalamus | thalamocortical | transthalamic | synapse physiology | circuit anatomy

Higher-order (HO) thalamic nuclei and their contributions to sensory processes remain poorly understood both in terms of the information they transmit to cerebral cortex and the effects they exert on specific cortical targets. First-order (FO) thalamic nuclei receive driving input from subcortical sources and act only as feedforward relays. On the other hand, HO thalamic nuclei may receive mixed driving inputs from the cortex and brainstem, and in turn project to primary sensory cortex and higher cortical areas. Therefore, the individual cells of HO thalamus may transmit information in the feedforward or feedback direction depending on their projection target and the source of relevant inputs that drive their activity. For instance, a transthalamic pathway from S1 through the HO somatosensory thalamic nucleus, posterior medial (POm), to S2 would be feedforward, but one from S2 through POm to S1 would be feedback.

Converging lines of evidence suggest that HO thalamic nuclei play an active role in early sensory processing in rodents and primates (1–5). For instance, POm has been shown to exert strong effects on S1 responses to whisker stimulation (6, 7), and it has been suggested that POm integrates incoming bottom-up input from the spinal trigeminal nucleus (SpV) with descending cortical inputs (8). A potential role for POm in integrating motor and sensory cues has been proposed (9–11), and it also regulates interactions between cortical areas (12, 13).

Similarly, damage to the HO visual thalamic nucleus, the pulvinar* (Pul), in humans and nonhuman primates has been associated with a range of visual and attentional deficits (14–16). Inactivation of Pul in primates or cats alters V1 responses to visual stimuli (17, 18), and the activity of Pul axons in V1 of mice can be used to predict motor actions and visuomotor discrepancies (19). The Pul has also been shown to regulate attentional selection in primates and enable functional transmission of information from one cortical area to another (18, 20), generating another parallel between POm and Pul and lending support to the notion that HO thalamic nuclei play a role in interpreting sensory cues in behavioral contexts (4). However, a more detailed appreciation of the underlying circuitry is required to understand the specific ways in which HO thalamus contributes to cortical processing.

## Significance

Neuroanatomical tracing provides just a partial picture of information flow in the brain, because excitatory synapses are not all equal. Some strongly drive postsynaptic targets to transfer information, whereas others weakly modulate their responsiveness. Here, we show conserved patterns of synaptic function across somatosensory and visual thalamocortical circuits in mice involving higher-order thalamic nuclei. These nuclei serve as hubs in transthalamic or cortico-thalamo-cortical pathways. We report that feedforward transthalamic circuits in the somatosensory and visual systems operate to efficiently transmit information, whereas feedback transthalamic circuits act to modulate their target areas. These patterns may generalize to other brain systems and show how methods of synapse physiology and molecular biology can inform the exploration of brain circuitry and information processing.

*The pulvinar in mice and rats has also been referred to as the lateral posterior nucleus (4).

We directly compared input and output features of the HO somatosensory nucleus, POm, with those of the HO visual nucleus, Pul, to clarify which aspects of functional organization are specific to each system or alternatively conserved across both. We asked two major questions of these HO pathways. The first question is: What effects do HO thalamocortical terminals exert on excitatory neurons at different levels of the cortical hierarchy? In particular, do POm and Pul drive or modulate targets in cortex? It has been recently shown that silencing Pul in cats results in different effects on sensory responses at different points of the visual cortical hierarchy (17). What differences in the synapse physiology at each target site might underlie this finding? The driver vs. modulator framework for classifying glutamatergic synapses using anatomical and physiological criteria has proven useful for parsing glutamatergic projections that can exert very different types of functional influence over postsynaptic targets (see reviews in 1 and 21). To apply the driver/modulator framework to HO thalamocortical projections in the visual and somatosensory systems of mice, we developed an optogenetics protocol in an in vitro slice preparation consistent with similar approaches using electrical stimulation (22, 23). We then evaluated physiological and pharmacological characteristics of HO thalamocortical synapses onto excitatory neurons in different layers of primary and secondary somatosensory cortex (S1 and S2) as well as in primary and higher visual areas (V1 and HVAs, mostly area LM). The somatosensory and visual systems both exhibited a similar divergence of synaptic properties between primary and higher cortical areas, wherein HO thalamus modulated S1 and V1 while strongly driving S2 and HVAs.

The second question is: Of the diverse cortical and subcortical inputs to HO thalamic cells, where does the activity relayed by HO thalamus to primary sensory cortex originate? We focused on the inputs to the POm → S1 and Pul → V1 pathways, because in both systems, evidence suggests that HO thalamic input to secondary areas are driven by layer 5 of primary sensory cortex in feedforward transthalamic pathways (12, 24), possibly in combination with subcortical inputs (25, 26). However, it is not known to what extent HO thalamic cells projecting to S1 or V1 carry signals from primary or higher sensory cortex, motor areas, subcortical sources, or a mixture. We addressed these questions using output-defined anatomical tracing in combination with optogenetic circuit mapping to reveal further similarities in the organization of the two systems.

These data reveal a previously undescribed form of transthalamic feedback from higher cortical areas to lower, running parallel to direct corticocortical feedback projections in both the somatosensory and visual systems; this arrangement is similar to transthalamic pathways connecting cortical areas in the feedforward direction (4). They also suggest that, whereas feedforward transthalamic projections appear to drive postsynaptic targets, feedback transthalamic projections modulate targets earlier in the cortical hierarchy. We find that these results in combination with other recent findings contribute insights into HO thalamocortical organization and information processing in sensory systems.

## Results

### HO Thalamocortical Projections Differentially Affect Primary vs. Higher Cortical Areas. We first developed an optogenetic stimulation approach to characterize HO thalamocortical physiology in acute slices, validated by comparison with previous approaches using electrical stimulation (see Fig. 1 and 22) and employing a slice preparation in which much of the

connectivity between thalamus and cortex is preserved (27). We confirm previous findings regarding the POm projection to S1 (22) and extend them by recording postsynaptic responses to POm stimulation from cells in layers 2–6 of S2. Furthermore, since a connected slice preparation is not readily available in the visual system due to the geometry of thalamocortical projections in the adult mouse (28), we extended the above observation to the visual system by using optogenetics to stimulate axons arising from Pul while recording from cells in layers 2–6 of V1 and HVAs (largely area LM, but also areas AM and AL) (*SI Appendix*, Table S1 and *Discussion*).

An important synaptic variable we measured was paired-pulse ratio (PPR), either depression or facilitation. However, several virally mediated optogenetics protocols appear to affect PPRs when terminals are directly photostimulated (11, 29). We thus adopted a strategy for measuring PPRs by photostimulating afferents via their axons >300 μm from the recorded cell and terminals, which ameliorated this problem (see below).

### Thalamocortical synaptic properties for POm projections to S1 and S2. Expressing ChR2-Venus by AAV injection in POm (while avoiding the neighboring FO nucleus VPm) (Fig. 1*A*) led to characteristic laminar distributions of labeled axons and terminals in S1 (most dense in layer 5a) and S2 (most dense in layer 4) (Fig. 1*B*). In mice with such expression, we made acute slices and established whole-cell recordings of putatively excitatory neurons in layers 2–6. In voltage clamp mode, excitatory postsynaptic currents (EPSCs) were recorded from many of these cells while applying 10 Hz focal laser stimulation through the microscope objective to measure the PPR. As noted above, laser stimulation targeted ChR2-expressing axons >300 μm from the recording site, recruiting the axons' action potential transmission without optically activating the terminals directly. In keeping with previous data, all POm synapses in S1 showed paired-pulse facilitation (i.e., the amplitude of the second evoked EPSC being larger than that of the first, leading to a PPR >1) with a mean PPR of $1.27 \pm 0.07$ (mean $\pm$ SEM throughout; n= 12 cells) (Fig. 1 *E* and *I*). By comparison, POm synapses in S2 evoked paired-pulse depression (i.e., the second EPSC amplitude being smaller than that of the first, leading to a PPR <1) with a mean PPR of $0.64 \pm 0.05$ ($n = 13$ cells). Thus, recorded PPRs were significantly different in S1 vs. S2 when pooling across all layers ($P = 3.9 \times 10^{-7}$, Mann Whitney $U$ test throughout unless otherwise specified) or when considering only cells in layers 2/3 ($n = 6$ cells in S1; $n = 8$ cells in S2, $P = 6.7 \times 10^{-4}$). As discussed further below, for comparison with previous studies of responses to FO thalamic stimulation in layers 2/3 of cortex, recordings in S2 focused on layers 2/3, but paired-pulse depression was observed in all layers (*SI Appendix*, Table S1 for data specific to each layer). In separate animals where the connection between thalamus and somatosensory cortex was entirely preserved, 10 Hz electrical stimulation of POm axons under otherwise identical recording conditions produced a similar divergence of PPR in S1 and S2 (Fig. 1*G*), suggesting that our optogenetic stimulation approach minimally altered release probability. All responses in cortex to 10 Hz stimulation were blocked by bath application of ionotropic glutamate receptor (iGluR) antagonists DNQX and AP5 and optogenetic responses had short latencies ($3.51$ ms $\pm 0.14$) consistent with previous measurements of monosynaptic responses to axonal stimulation of thalamocortical afferents (11). Initial EPSC amplitudes evoked were smaller for cells in S1 (12.0 pA $\pm 1.60$, $n = 12$ cells) than for those in S2 (37.8 pA $\pm 7.24$, $n = 13$ cells) ($P = 3.4 \times 10^{-4}$ when pooling across all layers, $P = 1.3 \times 10^{-3}$ for cells in
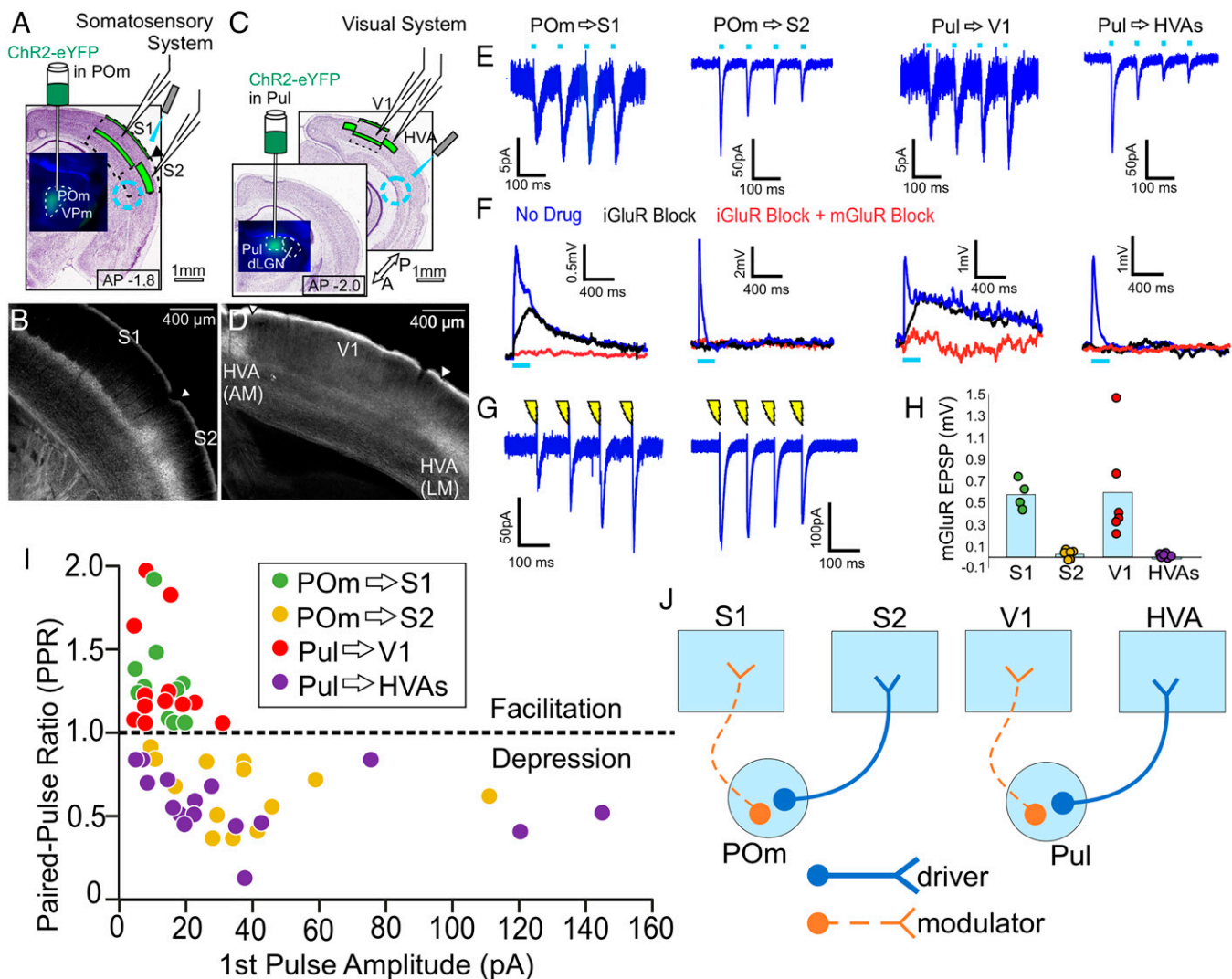
**Fig. 1.** HO thalamocortical synapses exert different effects on primary vs. higher cortical areas. (*A*) A schematic of experimental strategy to evaluate HO thalamocortical synapses in the somatosensory system. AAV9-pACAGW-ChR2-Venus was injected into the HO thalamic nucleus POm, allowing visualization and focal laser stimulation of POm axons in an acute slice during whole-cell recordings from S1 or S2. AP denotes rostrocaudal distance in mm from bregma throughout. (*B*) ChR2-Venus + POm axons densely innervate layer 5a of S1 and layers 2/3 and 4 of S2, showing a clear border. (*C*) Same experimental strategy as in (*A*), but evaluating HO thalamocortical synapses of the visual system by injecting AAV9-pACAGW-ChR2-Venus into Pul, allowing visualization and focal laser stimulation of Pul axons during whole-cell recordings from V1 or HVAs. (*D*) ChR2-Venus + Pul axons densely innervate layer 5a of V1 and layers 2/3 and 4 of HVAs, showing a clear border. (*E*) Example voltage clamp recordings from S1 and S2 during optogenetic stimulation of POm axons (10 Hz, 1 ms pulse duration, >300 μm away from the recording site), or from V1 or HVAs during stimulation of Pul axons also >300 μm away from the recording site. All 10 Hz responses blockable with iGluR blockers DNQX and APV. (*F*) Example current clamp recordings during high frequency stimulation over presynaptic terminals (83 Hz, 1-ms pulse duration) of the same HO thalamic axons as in (*E*). Blue traces are responses before the application of drugs. Black traces are during bath application of iGluR blockers DNQX and APV, and red traces are in the presence of iGluR blockers and group 1 mGluR blockers LY367385 and MPEP. (*G*) Example voltage clamp recordings from S1 and S2 during electrical stimulation of POm axons (10 Hz, 0.1-ms duration) in a connected thalamocortical slice. (*H*) mGluR-dependent responses to high frequency stimulation in S1 (*n* = 4 cells), S2 (*n* = 6), V1 (*n* = 6), and HVAs (*n* = 6). mGluR responses in S1 (0.58 mV ± 0.07) and S2 (0.03 mV ± 0.02) are significantly different from each other (*P* = 9.5 × 10$^{-3}$, Mann-Whitney *U* test throughout unless otherwise specified), and mGluR responses in V1 (0.59 mV ± 0.19) and HVAs (-0.015 mV ± 0.028) are significantly different from each other (*P* = 2.2 × 10$^{-3}$). Here and later figures, bars represent the mean while dots represent the data for individual cells. (*I*) Scatterplot showing relationship of paired-pulse ratio (second EPSC amplitude/first EPSC amplitude) and amplitude of the first evoked EPSC in a train for thalamocortical inputs to cortical neurons. Data include cells in S1 (*n* = 12, green), S2 (*n* = 13, tan), V1 (*n* = 12, red), and HVAs (*n* = 16, purple). PPRs in S1 (1.27 ± 0.07, mean ± SEM throughout) and S2 (0.64 ± 0.05) are significantly different from each other (*P* = 3.9 × 10$^{-7}$), and PPRs in V1 (1.30 ± 0.09) and HVAs (0.57 ± 0.05) are significantly different from each other (*P* = 6.6 × 10$^{-8}$). Response amplitudes in S1 (12.0 pA ± 1.60) and S2 (37.8 pA ± 7.24) are significantly different from each other (*P* = 3.4 × 10$^{-4}$), and response amplitudes in V1 (13.3 pA ± 2.35) and HVAs (38.8 pA ± 10.21) are significantly different from each other (*P* = 2.0 × 10$^{-2}$). (*J*) Summary of data interpreted in the context of glutamatergic drivers and modulators.

layers 2/3 only [*n* = 6 cells in S1, *n* = 8 cells in S2]) (Fig. 1 *E* and *I*), despite no significant difference in input resistances across areas (183 MΩ ± 17.4 in S1 vs. 166 MΩ ± 9.44 in S2, consistent with previous recordings in adult mice) (11).

We also verify the observation that the stimulation of ChR2 terminals directly (rather than remotely stimulating the axons) results in an artificial synaptic depression in some pathways. In particular, the facilitating responses observed here with axonal

activation became depressing when focal stimulation was delivered over the terminals and postsynaptic cell body (*SI Appendix*, Fig. S1A). With axonal stimulation >300 μm from the recorded cell, we always measured facilitation in S1 and depression in S2. In depressing pathways (e.g., when recording in S2 or recordings below), terminal stimulation did not produce depression that significantly differed from that seen with axonal stimulation.

In current clamp mode, high frequency optogenetic stimulation (83 Hz) was delivered over presynaptic terminals to test for the activation of a slow metabotropic glutamate receptor (mGluR) dependent excitatory postsynaptic potentials (EPSPs) (Fig. 1*F*). In all completed tests during S1 recordings, high frequency stimulation evoked slow EPSPs (mean amplitude 0.58 mV ± 0.07, $n = 4$ cells), which were blocked by group I mGluR antagonists (LY367385 and MPEP) and were dependent on repetitive stimulation (30) (*SI Appendix*, Fig. S1*B*). mGluR-dependent EPSPs were absent in all recordings in S2 (0.03 mV ± 0.02, $n = 6$ cells, $P = 9.5 \times 10^{-3}$) (Fig. 1*H*).

Therefore, properties of synapse physiology and pharmacology with known functional implications diverged notably for POm synapses in S1 vs. S2, consistent with their characterization as glutamatergic modulators and drivers, respectively (Fig. 1 *J, Left*).

***Thalamocortical synaptic properties for Pul projections to V1 and HVAs.*** We then applied the same experimental approaches to the visual system. We expressed ChR2-Venus by AAV injection limited to Pul while avoiding delivering ChR2-Venus to neighboring structures, especially the lateral geniculate nucleus (dLGN) (Fig. 1*C*). As with the POm thalamocortical projections, Pul axons densely innervate layer 5a of V1 and layer 4 of HVAs (Fig. 1*D*). Again, putatively excitatory cells were targeted for whole-cell recordings. For all cells recorded in layers 2–6 in V1, responses to 10 Hz stimulation of ChR2-axons >300 um from the recorded cells evoked facilitating responses, with a mean PPR of 1.30 ± 0.09 ($n = 12$ cells) (*SI Appendix*, Table S1), while those recorded in layers 2–6 of HVAs always evoked depressing responses (mean PPR 0.57 ± 0.05 $n = 16$ cells) (Fig. 1 *E* and *I*). PPRs were significantly different in V1 than HVAs when pooling across all layers ($P = 6.6 \times 10^{-8}$) or when comparing only cells in layers 2/3 ($n = 5$ cells in V1, $n = 8$ cells

in HVAs, $P = 1.6 \times 10^{-3}$). Initial EPSC amplitudes were smaller in V1 cells (13.3 pA ± 2.35) compared with those in HVAs (38.8 pA ± 10.21, $P = 2.0 \times 10^{-2}$ pooling across all layers) (Fig. 1 *E* and *I*) despite no significant difference in input resistances across areas (194 MΩ ± 20.2 for V1 vs. 176 MΩ ± 14.5 for HVAs) and were blocked by bath application of iGluR antagonists. Finally, high frequency stimulation over presynaptic terminals evoked slow mGluR-dependent EPSPs in recordings in V1 (mean amplitude 0.59 mV ± 0.19, $n = 6$) but not in HVAs (−0.015 mV ± 0.028, $n = 6$, $P = 2.2 \times 10^{-3}$; Fig. 1 *F* and *H*).

Overall, the visual system showed the same pattern as the somatosensory system, with properties of synapse physiology and pharmacology differing substantially between Pul synapses in V1 vs. HVAs, consistent with the hypothesis that Pul synapses in V1 act as glutamatergic modulators while those in HVAs act as drivers (Fig. 1*J*).

**POm and Pul Cells Projecting to Primary Sensory Cortex Are Innervated by Layer 5 Cells from Multiple Cortical Areas.** Since thalamocortical projections from the POm and Pul evoke different postsynaptic responses at different points on the sensory cortical hierarchy, we asked: What are the driving inputs to POm and Pul cells projecting to these different cortical targets? Evidence suggests that HO thalamic input to secondary areas in both systems is driven by layer 5 of primary sensory cortex forming feedforward transthalamic pathways (11, 12, 24), possibly integrated with subcortical inputs (25, 26). Because this input-output relationship has already been explored, we wanted to identify the driving inputs to POm and Pul cells projecting to primary sensory cortices. We first used an anatomical tracing technique to identify putative inputs to POm → S1 and Pul → V1 cells. We used an output-defined G-deleted rabies tracing strategy (31, 32), which retrogradely
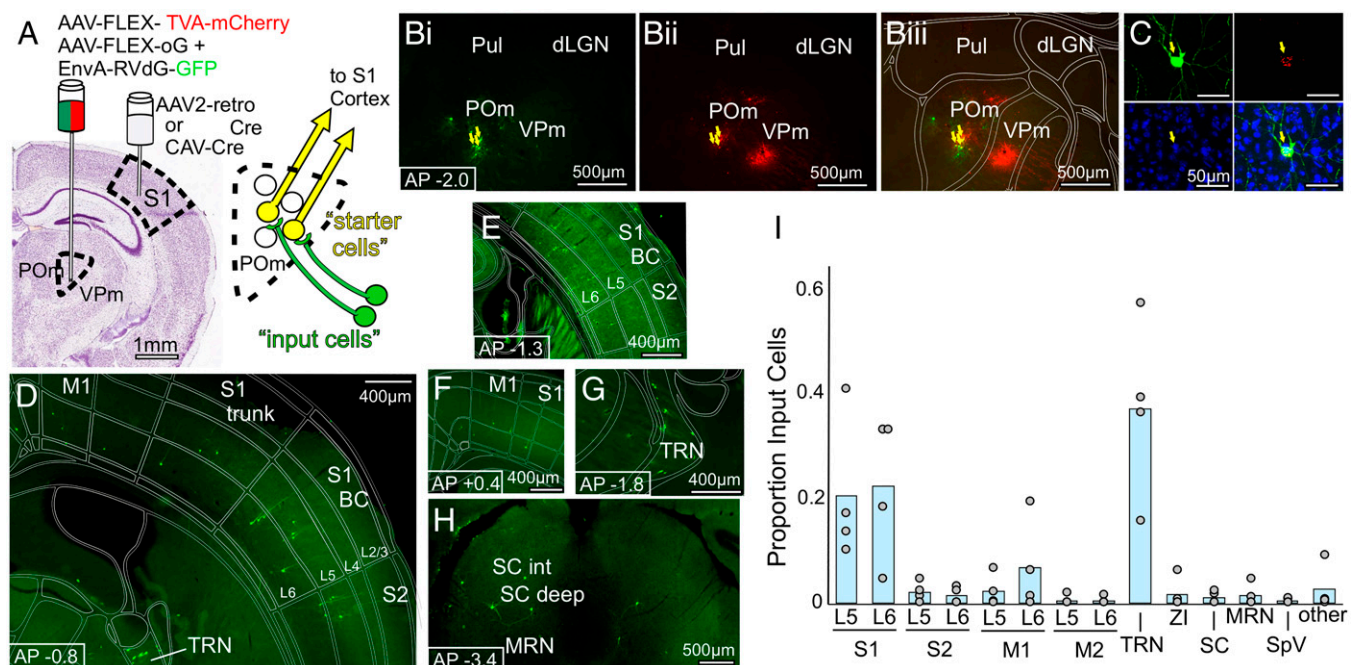


**Fig. 2.** Retrograde transsynaptic tracing of inputs to the POm → S1 pathway. (*A*) Schematic of the anatomical labeling strategy for labeling presynaptic inputs to the POm → S1 pathway (see *Results* and *Materials and Methods* for details) (*B*) Representative images of POm, with GFP+ (*B, i*) and mCherry+ (*B, ii*) "starter" cells double labeled (yellow arrows) in POm only (overlay in *B, iii*). (*C*) Higher magnification image of a double labeled "starter" cell in POm, *Top Left*, GFP; *Top Right*, mCherry; *Bottom Left*, DAPI; *Bottom Right*, overlay. (*D–H*) Representative epifluorescence images of GFP+ presynaptic "input" cells, projecting to the POm → S1 pathway. Cortical layers are labeled L2/3, L4, etc. Abbreviations: BC, barrel cortex S1, TRN, thalamic reticular nucleus; SC int, SC intermediate layers; MRN, midbrain reticular nucleus. (*I*) Location of presynaptic GFP+ input cells as a proportion of the number of input cells found in each mouse ($n = 4$ animals). Of note are labeled input cells in layer 5 of several cortical areas and a lack of labeling in brainstem nucleus SpV.

and transsynaptically labels inputs to a particular subpopulation of cells as defined by projection identity (see *Materials and Methods* for details).

***Identifying inputs to the POm → S1 pathway.*** By delivering cre to the POm → S1 population (via injection of AAVretro-cre or CAV-cre in S1), as well as cre-dependent rabies machinery (via AAV-FLEX-TVA-mCherry and AAV-G injection in POm), we rendered the POm → S1 population receptive to subsequent pseudotyped rabies infection (i.e., RV-GFP), causing them to be double-labeled with mCherry and GFP. Only the double-labeled POm → S1 "starter cells" had the necessary receptor to accept rabies virus infection, and also had the rabies glycoprotein (G) necessary to transsynaptically label their presynaptic inputs (Fig. 2*A*). After validating that double-labeled "starter cells" were only present in POm, we searched for distant GFP-labeled presynaptic "input cells."

Due to well-known difficulties with leaky expression of TVA-mCherry and potential for false positives and negatives using this approach (32), we developed a protocol with limited viral volumes to generate sparse labeling. We then did as follows: we manually screened each brain section; we discarded data from any animals with starter cells in the neighboring FO thalamic nucleus projecting to the same sensory cortical areas; we carefully assessed controls lacking cre recombinase (*SI Appendix,* Figs. S2 *D–F* and S3 *D–F*); and we validated key findings using optogenetics-based methods (below). Even with care taken to ensure the quality of anatomical data from G-deleted-rabies experiments, there are still many cell-type biases inherent to viral tracing techniques. Therefore, we regard these results as qualitatively informative regarding which areas project to the targeted POm → S1 and Pul → V1 subpopulations, and indeed they guided our optogenetics experiments described below, but they are not reliable for providing quantitative comparisons of input areas.

Inhibitory inputs from thalamic reticular nucleus (Fig. 2*G*) and zona incerta were labeled, as well as the layer 6 corticothalamic cells (Fig. 2 *D–F*) known to exert modulatory rather than driving input to thalamocortical cells (4, 26, 33). Among expected inputs, negligible label was seen in the spinal trigeminal nucleus (SpV) (two cells in two animals, and no label in two animals) (Fig. 2*I*), which is known to relay whisker-related signals to POm (34, 35).

Prominent contributions of input to the POm → S1 pathway were found in layer 5 cells of S1 itself (Fig. 2 *D* and *E*) as well as in layer 5 of S2 (Fig. 2*D*) and M1 (Fig. 2*F*); other inputs were also seen scattered in other areas (Fig. 2*I*). Because the layer 5 input to thalamus has been shown in many studies to be a strong, driving input (below) (4, 26, 33), we used these anatomical results to direct further experiments testing whether the layer 5 cells identified by this transsynaptic tracing approach (those in S1, S2, and M1) indeed drive POm cells projecting to S1. We also explored the surprising lack of inputs from SpV (see below).

***Identifying inputs to the Pul → V1 pathway.*** We next performed the analogous anatomical experiment aimed to identify inputs to Pul → V1 cells (Fig. 3*A*). We limited cre expression to the Pul → V1 subpopulation by delivering it via a retrograde viral injection in V1, then cre-dependent rabies machinery tagged with mCherry was delivered to the Pul, followed by RV-GFP, leaving double-labeled Pul → V1 "starter cells" (Fig. 3*B*), and distant GFP-only presynaptic "input cells."

Again, expected inputs were found in the inhibitory cells of thalamic reticular nucleus and zona incerta, as well as layer 6 of V1 and HVAs (Fig. 3 *C, D,* and *G*). Inputs from layer 5 of cortex were again observed in both V1 (Fig. 3 *C, D,* and *F*) and HVAs (Fig. 3 *C, D,* and *G*); SC also had cells innervating Pul → V1 (Fig. 3*E*). Notably, Pul includes at least 2 populations of
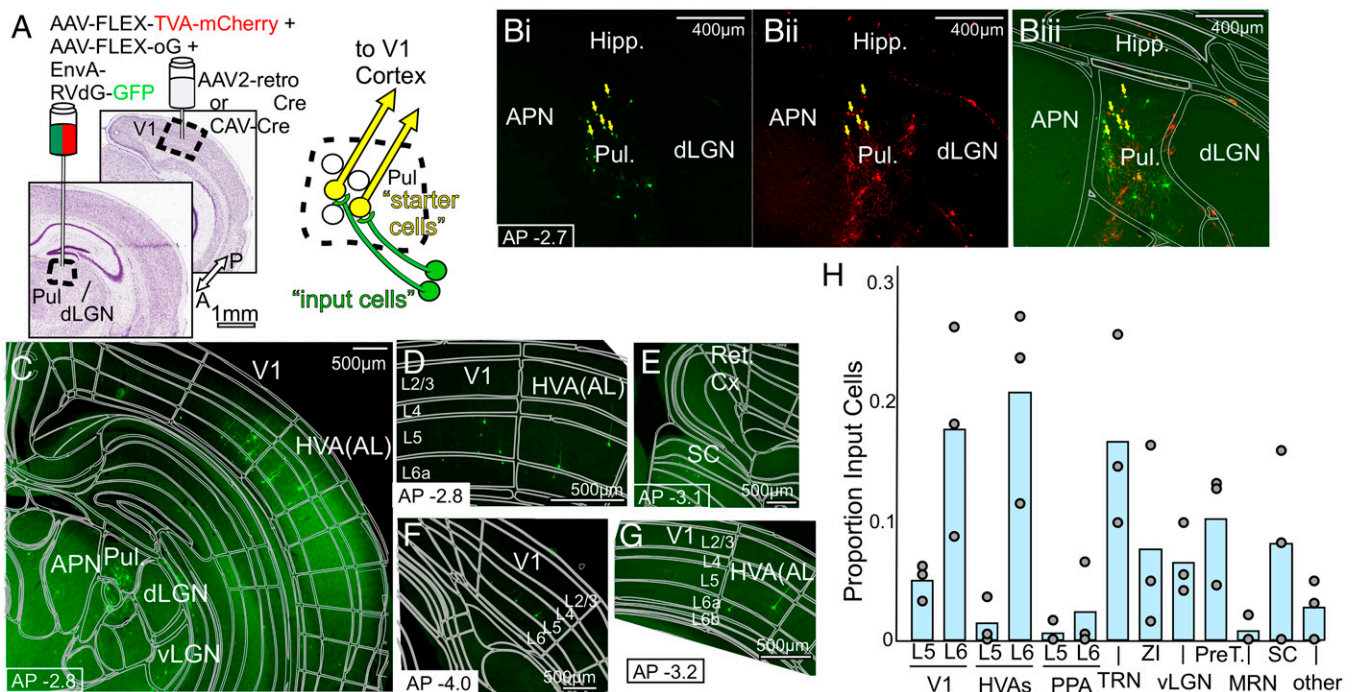


**Fig. 3.** Retrograde transsynaptic tracing of inputs to the Pul → V1 pathway. (*A*) Schematic of the anatomical labeling strategy for labeling presynaptic inputs to the Pul → V1 pathway (see *Results* and *Materials and Methods* for details) (*B*) Representative images of Pul, with GFP+ (*B, i*) and mCherry+ (*B, ii*) cells double labeled (yellow arrows) in Pul only (overlay in *B, iii*). (*C–G*) Representative epifluorescence images of GFP+ presynaptic "input" cells, projecting to the Pul → V1 pathway. Cortical layers are labeled L2/3, L4, etc. Abbreviations: APN, anterior pretectal nucleus, Ret. Cx, retrosplenial cortex. (*H*) Location of presynaptic GFP+ input cells as a proportion of the number of input cells found in each mouse (*n* = 3 animals). Of note are labeled input cells in layer 5 of several cortical areas and SC cells labeled in two animals, although missing in an animal with a slightly more anterior Pul injection.

Pul → V1 cells, one in the striate-recipient rostral pulvinar and one in the SC-recipient caudal and lateral Pul (36, 37). Slight variation in the anterior-posterior position of the rabies virus injections in Pul likely accounts for differences between animals in these results, with a slightly more anterior injection in one animal (*SI Appendix*, Fig. S3 *B*, *i*) resulting in more labeled inputs coming from layer 5 of higher visual areas and a total lack of SC inputs, whereas a more posterior injection in another animal (*SI Appendix*, Fig. S3 *B*, *ii*) favored the labeling of SC inputs, and an intermediate position in a third animal (thus targeting both Pul → V1 populations) labeled both inputs from layer 5 of HVAs as well as SC inputs (Fig. 3*H*). Layer 5 of V1 provided input to Pul → V1 cells in all animals, in agreement with recent results that V1 can strongly drive some SC-recipient cells in the lateral Pul (26).

**Layer 5 of Multiple Cortical Areas Can Drive Transthalamic Feedback to S1 and V1.** We used an optogenetics-assisted circuit mapping approach in layer 5 cre transgenic mice (Rpb4-cre) to validate the above anatomical findings and the expectation that layer 5 corticothalamic terminals should be strong drivers of thalamic activity (4, 26, 33). Specifically, a retrograde label (Fluororuby) was injected into all layers of S1 or V1, while an AAV expressing cre-dependent (FLEX) ChR2-eYFP was injected into

candidate input cortical areas identified above. We then prepared acute slices in which we could target for whole-cell recording the retrolabeled POm → S1 or Pul → V1 cells while optogenetically stimulating layer 5 axons from the candidate input area and thereby verify and describe the properties of these putative inputs. Typical patterns of labeling in thalamus are shown in *SI Appendix*, Fig. S4. Note that in many cases, retrograde labeling looks quite sparse in HO thalamus, especially Pul, consistent with previous reports (19). However, even in these cases, at higher magnification retrogradely labeled cells are visible, as in Fig. 4 *A*, *ii*, *Bottom*.

**Transthalamic pathways innervating S1.** While making whole-cell recordings from retrolabeled POm → S1 cells, focal laser stimulation of ChR2 axons or terminals from layer 5 of S1, S2, or M1 evoked depressing EPSCs (*n* = 13 cells, 4 cells, and 4 cells, respectively, PPRs = 0.57 ± 0.08, 0.72 ± 0.14, 0.59 ± 0.07, Fig. 4 *A*–*C*), dependent on iGluRs with no evidence of a postsynaptic contribution of mGluRs (*SI Appendix*, Fig. S1*E*), with a mixture of large and small amplitudes (104 pA ± 20.7, 11.2 pA ± 5.61, 21.9 pA ± 9.17) (*SI Appendix*, Fig. S1*C*), all consistent with previous observations of layer 5 input to thalamus (1, 4, 11, 26, 33). In the case of all layer 5 corticothalamic projections studied, optogenetic stimulation over either
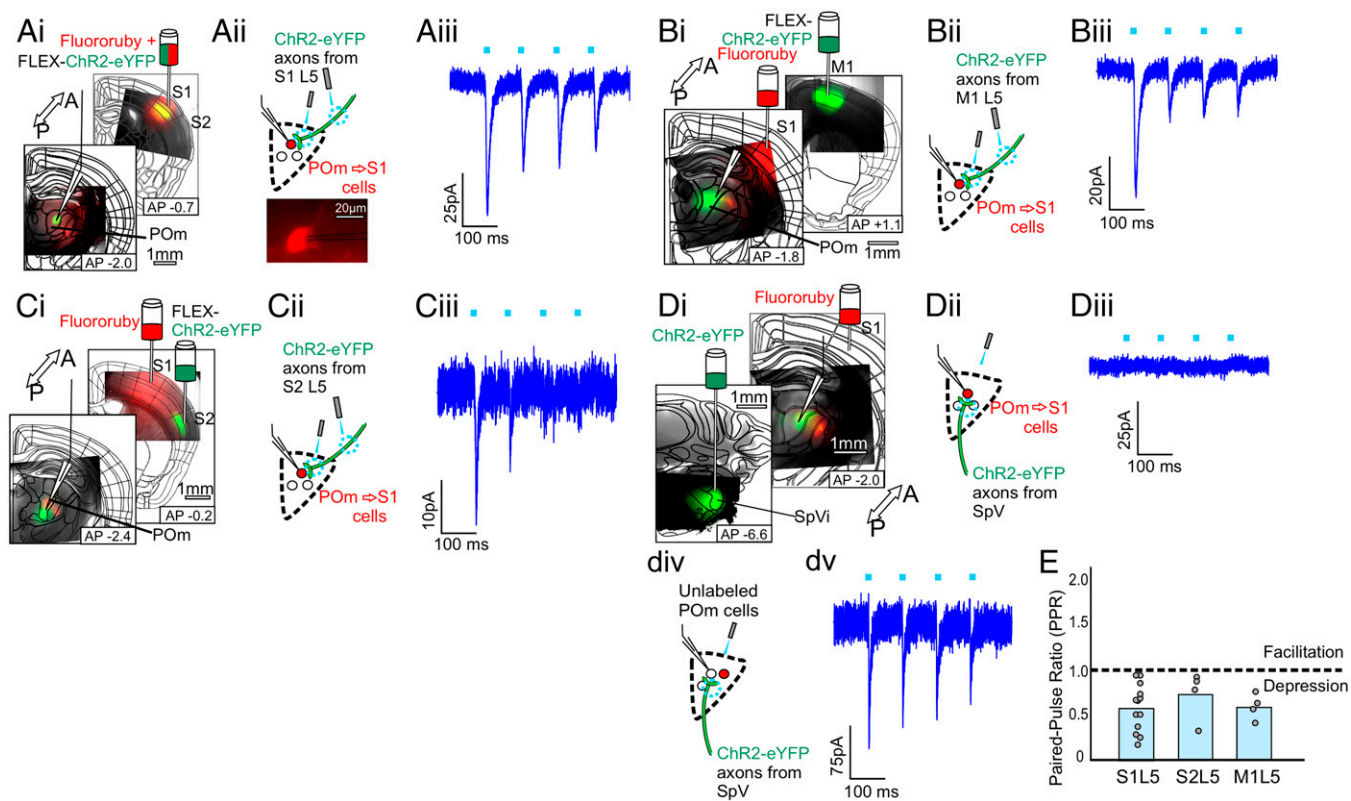


**Fig. 4.** Layer 5 of S1, S2, or M1 can drive the POm → S1 pathway. (*A*, *i*) A schematic of the experimental strategy to validate layer 5 input from S1 to the POm → S1 pathway and epifluorescence images of injection and recording sites. A retrograde label (Fluororuby) was injected into S1 to label the POm → S1 cells (as well as other cells projecting to S1, e.g., in VPm) and an AAV expressing cre-dependent ChR2 (AAV9-pAAV-EF1a-DIO-hChR2(H134R)-EYFP-WPRE-HGHpA) was injected into the candidate input area, in this case S1 itself, in layer 5 cre (RBP4-cre) transgenic animals. The white recording pipette drawn over the epifluorescence image points to the recording site in POm, where red retrograde label and green layer 5 axons overlap. (*A*, *ii*) A schematic of the recording configuration. Labeled POm → S1 cells as shown (*Bottom*) were targeted for whole-cell recordings while photostimulating axons and/or terminals from layer 5 of S1. (*A*, *iii*) Example voltage clamp recording of a POm → S1 cell during 10 Hz photostimulation of axons from L5 of S1. All layer 5 responses were blocked with iGluR antagonists DNQX and APV (*SI Appendix*, Fig. S1*E*). (*B*, *i*, *ii*) Same as in (*A*), but the cre-dependent ChR2 was expressed in layer 5 of M1. (*B*, *iii*) Example voltage clamp recording from POm → S1 cell during 10 Hz photostimulation of axons from L5 of M1. (*C*, *i*, *ii*) Same as in (*A*) and (*B*), but the cre-dependent ChR2 was expressed in layer 5 of S2. (*C*, *iii*) Example voltage clamp recording from POm → S1 cell during 10 Hz photostimulation of axons from L5 of S2. (*D i*, *ii*) Same as in (*A*)–(*C*), except ChR2 was expressed in SpV (interpolaris region). (*D*, *iii*) Example trace from a retrolabeled POm → S1 cell during photostimulation of axons from SpV. These failed to evoke EPSCs onto labeled POm → S1 cells (*n* = 12 cells). (*D*, *iv*, *v*) Example traces from an unlabeled POm cell of unknown projection identity during SpV photostimulation (*n* = 3). (*E*) PPRs (second EPSC amplitude/first EPSC amplitude) for responses of retrolabeled POm → S1 cells to photostimulation of layer 5 of S1 (*n* = 13 cells), S2 (*n* = 4), or M1 (*n* = 4).

terminals or distant axons produced paired-pulse depression (*SI Appendix,* Fig. S1*A*).

***SpV innervation of POm.*** We had seen that SpV was not strongly labeled by transsynaptic retrograde tracing as a source of input to the POm → S1 subpopulation (Fig. 2*I*). Consistent with that finding, despite the dense innervation of POm by ChR2-eYFP axons from SpV (Fig. 4 *D, i*), while optogenetically stimulating SpV axons, we were not able to record EPSCs from retrolabeled POm → S1 cells, only from unlabeled cells in POm of uncertain projection identity (*n* = 5 cells, Fig. 4*D*).

These results fail to provide evidence for a feedforward pathway from SpV through POm to S1 but do confirm the existence of transthalamic feedback pathways whereby layer 5 of S1, S2, and M1 drive POm → S1 cells, which in turn modulate activity in S1.

***Transthalamic pathways innervating V1.*** We used the same approach as in the somatosensory system to study the analogous circuits in the visual system. Thus, a retrograde label was injected into all layers of V1, while cre-dependent ChR2 was expressed in layer 5 of candidate input areas V1 and the HVA LM, the mouse cortical area most similar to V2 (see *Discussion*) (Fig. 5). When targeting for whole-cell recording the retrolabeled Pul → V1 cells and optogenetically stimulating layer 5 axons from V1 or LM, we observed similar depressing EPSCs (*n* = 9 cells and 5 cells, respectively, PPRs = 0.60 ± 0.04 and 0.39 ± 0.14) (Fig. 5 *A–C*) dependent on iGluRs and no evidence of postsynaptic mGluRs, with a mixture of small and large amplitudes (16.4 pA ± 4.68, 21.3 pA ± 6.81) (*SI Appendix,* Fig. S1*D*). These results confirm the existence of a transthalamic feedback pathway whereby layer 5 of V1 and LM drive Pul → V1 cells that in turn modulate activity in V1.

## Discussion

**Thalamocortical Drivers vs. Modulators.** We found many similarities in the organization of HO thalamocortical circuitry in the somatosensory and visual systems (see Fig. 6). First, HO thalamic terminals synapsing onto excitatory cells in S1 and V1 evoke small, facilitating EPSCs reflecting a low initial probability of neurotransmitter release (38), and when stimulated at high frequency, evoke mGluR-dependent slow EPSPs, properties of glutamatergic modulator synapses (1, 4, 39). This confirms and extends earlier work showing the same features for HO thalamic input to primary somatosensory and auditory cortices (22, 23). By comparison, HO thalamic terminals in higher cortical areas S2 and HVAs (with most such data deriving from LM) evoked stronger, depressing responses dependent on iGluRs only, consistent with descriptions of glutamatergic driver synapses (1, 4, 39).

The observed pattern of physiological and pharmacological properties reported here has been a central part of the driver/modulator framework for classifying glutamatergic synapses. Within that framework, our data suggest HO thalamocortical projections modulate activity in S1 and V1, while driving activity in higher cortical areas. The underlying hypothesis for the functional significance of this is as follows: driving projections
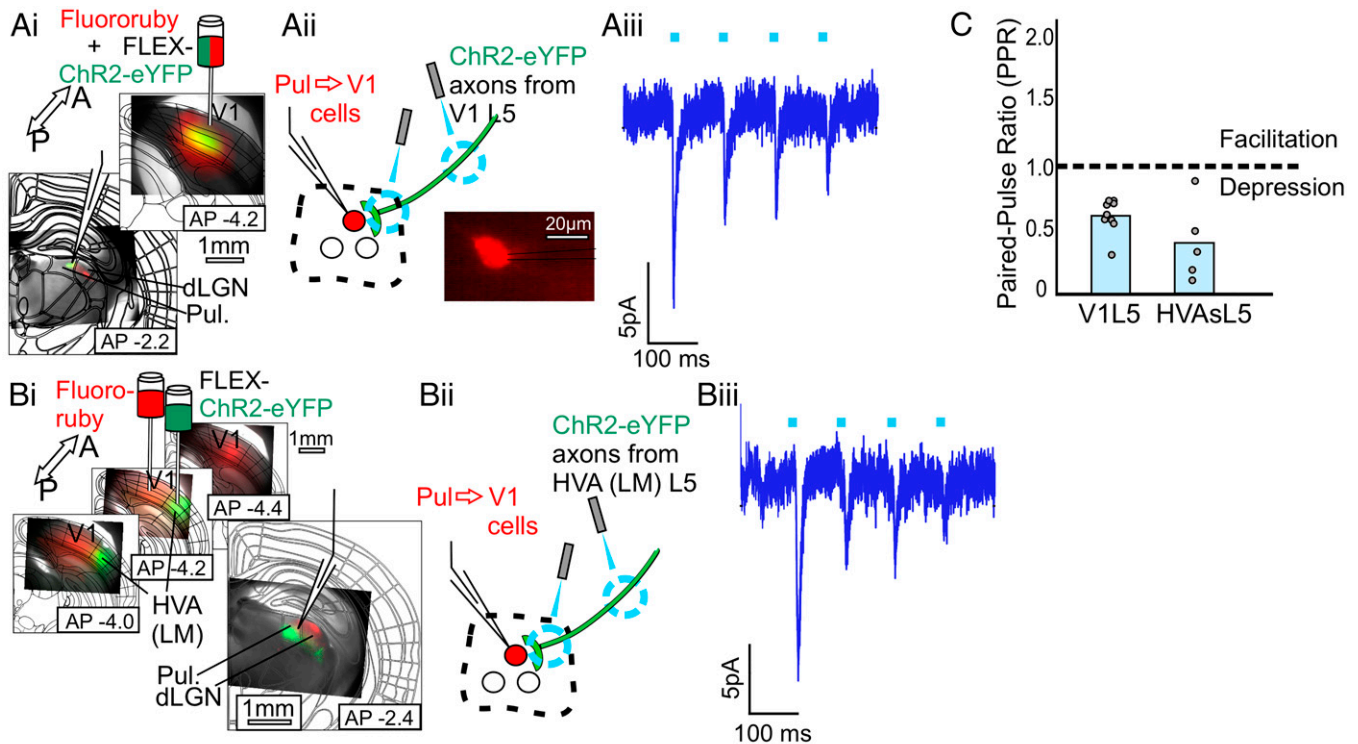


**Fig. 5.** Layer 5 of V1 or HVA LM can drive the Pul → V1 pathway. (*A, i*) A schematic of the experimental strategy to validate layer 5 input from V1 to the Pul → V1 pathway and epifluorescence images of injection and recording sites. A retrograde label (Fluororuby) was injected into V1 to label the Pul → V1 cells (as well as other cells projecting to V1, e.g., in LGN) and an AAV expressing cre-dependent ChR2 (AAV9-pAAV-EF1a-DIO-hChR2(H134R)-EYFP-WPRE-HGHpA) was injected into the candidate input area, in this case V1 itself, in layer 5 cre (RBP4-cre) transgenic animals. The white recording pipette drawn over the epifluorescence image points to the recording site, where red retrograde label and green layer 5 axons overlap. (*A, ii*) A schematic of the recording configuration. Labeled Pul → V1 cells as shown (*Bottom Right*) were targeted for whole-cell recordings while photostimulating axons and/or terminals from layer 5 of V1. (*A, iii*) Example voltage clamp recording of a Pul → V1 cell during 10 Hz photostimulation of V1L5. All layer 5 responses were blockable with iGluR blockers DNQX and APV (*SI Appendix,* Fig. S1*E*). (*B, i, ii*) Same as in (*A*), but the cre-dependent ChR2 was expressed in layer 5 of HVA LM. *B, iii:* Example voltage clamp recording from a Pul → V1 cell during 10 Hz HVAsL5 photostimulation. (*C*) PPRs (second EPSC amplitude/first EPSC amplitude) for responses of retrolabeled Pul → V1 cells to photostimulation of layer 5 of V1 (*n* = 9 cells) or HVA LM (*n* = 5).
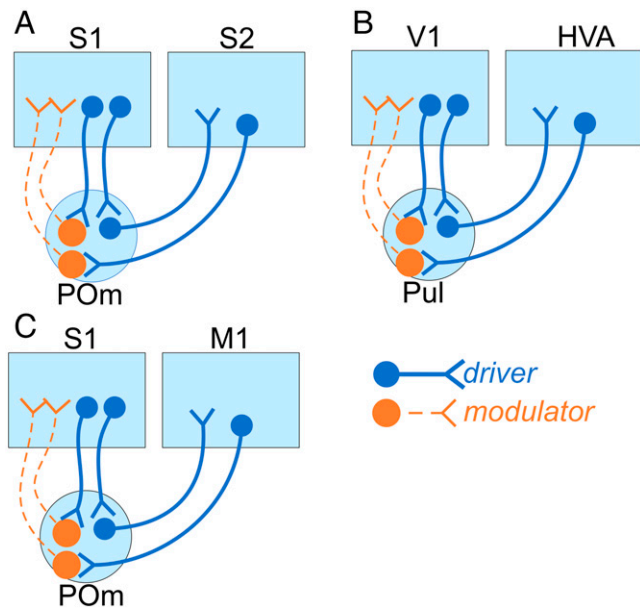
**Fig. 6.** Summary of main conclusions. In the feedforward direction, transthalamic pathways from S1 to S2 (*A*), V1 to HVAs (*B*), or S1 to M1 (*C*), all drive postsynaptic targets. Additionally, all inputs from layer 5 of cortex to HO thalamus are driver. However, the thalamocortical projections to primary cortical areas are modulatory, and are themselves driven by layer 5 of cortex in both reciprocal feedback pathways (layer 5 of S1 → POm → S1 and layer 5 of V1 → Pul → V1) as well as in transthalamic feedback from higher cortical areas to lower (layer 5 of S2 → POm → S1, layer 5 of M1 → POm → S1, and layer 5 of HVA LM → Pul → V1). Taken together, these data suggest that feedforward transthalamic pathways are mainly information-bearing, whereas feedback transthalamic pathways serve mainly a modulatory role.

provide temporally precise excitation well suited to the efficient transfer of information and have been shown in many cases to do so [examples in (26, 40), reviewed in (1, 4)]. Glutamatergic modulatory inputs are so named because their effects resemble those of classical neuromodulators; these exert modulatory influence, likely affecting how postsynaptic targets process driver inputs (1, 4).

Along with PPRs, response amplitudes, and mGluR-dependent conductances, the size of synaptic terminals has also been used as an important criterion for the driver/modulator framework. Driver pathways form larger presynaptic terminals than do modulatory pathways (11, 22, 23, 41, 42). Data presented here are consistent with these previous studies of thalamocortical terminal sizes. Pul terminals in V1 have generally been described as smaller than those in HVAs (37), and POm terminals in S1 are smaller than those in S2 (22).

**Differences between FO and HO Driving Pathways.** It is worth noting that the FO projection in the somatosensory and auditory systems (i.e., VPm → S1 and MGBv to A1) provide only driver input to the cells in layers 4–6, but for cells in layers 2/3, most receive modulator input, and the rest, driver (23). Consistent with this physiology, terminals from VPm in S1 were found to be smaller on average in layers 2/3 than in layers 4–6 (23). For the purpose of comparing FO vs. HO driving pathways, we acquired data from all layers 2–6 with emphasis on layers 2/3, and we found a very different pattern for the HO thalamocortical inputs to layers 2/3 of higher cortical areas. That is, HO thalamocortical input to all of the cells in layers 2/3 of S2 and HVAs were driver in nature [8 of 8 cells in layers 2/3 of S2 and 8 of 8 cells in layers 2/3 of HVAs, a significant difference from the driver/modulator ratio predicted by

findings in the VPm → S1 and MGBv → A1 pathways in (23), $P = 3.95 \times 10^{-26}$, $\chi^2$ test with Yates correction]. Consistent with that result, we recently showed that POm terminals in layer 4 of S2 (classical drivers) are not significantly larger than those in layers 2/3 (43). This distinction between FO and HO driving projections is not without precedent, due to the recent finding that the inputs from POm to M1 in all layers, including layers 2/3, are exclusively driver (11). Therefore, it may be a pattern common to other cortical circuitry that FO thalamic input strongly drives layer 4 and provides mixed inputs to layers 2/3 of primary cortical areas while HO thalamic input to higher cortical areas provides uniformly driving input to all layers.

**Technical and Experimental Considerations.** In our experiments using ChR2 to stimulate HO thalamic axons in cortex, we coactivated many individual thalamocortical afferents, and therefore postsynaptic responses may represent combined responses, where responses to a minority of synapses of one type could be overwhelmed by those of the other type. That is, what we see as a driver (or modulator pathway) could contain small modulator (or driver) components. While possible in some cases, this type of error is unlikely to strongly affect our results for the following reasons. If a mostly driver pathway contained a significant representation of modulator inputs, we would expect to see measurable mGluR-dependent responses, which were never seen in our recordings from S2 or HVAs. A more likely scenario would be missing a sparse driver input among a mostly modulator pathway, since driver synapses are generally a smaller proportion of cortical synapses. However, the distribution of EPSC amplitudes across areas suggests that this did not happen to any appreciable extent in our recordings in S1 and V1, since these amplitudes were all quite small. Thus, while we cannot rule out some mixing of input types, if such contamination exists it is functionally meager.

Area LM was chosen as the extrastriate cortical area of mice to represent "higher visual areas," because LM is the main downstream target of V1 (44), is considered hierarchically next above V1 (44, 45), and thus most closely resembling S2 hierarchically. Most cortical recordings reported here in HVAs were made in LM, but Pul stimulation evoked similar responses in AL [another intermediate or secondary area (44), and a recipient of a feedforward transthalamic pathway from V1 through Pul (24)] and area AM [described as near the top of the cortical hierarchy (45)] (*SI Appendix*, Table S1).

Last, this project focused on thalamocortical synapses onto putative excitatory neurons, and it is important to note that projections from HO thalamus to primary sensory cortices also target inhibitory interneurons, particularly through their axon terminations to layer 1 (37, 46), forming another, likely closely related mechanism for HO thalamic control of cortical activity. However, it was recently shown that the projection from POm to S2 targets only excitatory neurons (43), so this feature too may differ depending on hierarchical position or other circuit demands.

**Sensory Role of Higher-Order Thalamic Projections to Cortex.** The current results complement work exploring HO thalamic contributions to sensory responses in somatosensory and visual cortex. Zhang et al. (6) recently showed that inactivating POm during whisker stimulation does not disrupt the initial sensory response in layers 2/3 of S1 (presumably dependent on driver projections from VPm) but abolishes persistent activity that typically lasts for hundreds of milliseconds, presumably

dependent on the modulatory POm → S1 pathway, and possibly the mGluR conductances described here, which act over a similar timescale. Similarly in the visual system, deSouza et al. (17) recently showed in the cat that silencing Pul altered sensory responses less in V1 than in a HVA, consistent with the proposed modulator/driver roles of pulvinar synapses in V1 vs. HVAs.

**Layer 5 Cortical Inputs to POm → S1 and Pul → V1.** With regard to layer 5 cortical inputs to the POm → S1 and Pul → V1 pathways, transthalamic pathways between two separate cortical areas in the feedback direction had never been described before. We add to recent evidence showing the existence of reciprocal loops between a primary sensory cortical area and HO thalamus (45, 47, 48), wherein HO thalamic cells projecting to one area receive input from layer 5 of that same area. Given that HO thalamic projections to S1 and V1 appear modulatory, these reciprocal loops do not violate Francis Crick's no-strong-loops hypothesis, stipulating that closed driver-driver loops are unlikely to exist in the brain since they would cause runaway excitation (49). It remains unclear if such reciprocal loops in thalamocortical processing are always modulatory in nature or if some indeed violate Crick's hypothesis. As noted in the Introduction, we refer to transthalamic pathways connecting different cortical areas as "feedforward" or "feedback," depending on the direction of communication given the hierarchical relationship of the two relevant cortical areas, which seems intuitive. However, we more cautiously refer to reciprocal transthalamic pathways terminating in the area from which they arise as feedback (e.g., S1L5 → POm → S1), since POm does not clearly contribute new subcortical information to S1 via this route, but the distinction between feedforward and feedback becomes much less clear in this case, especially when considering that some individual POm and Pul cells have recently been shown to integrate driving inputs from more than one source (13, 26).

As shown here and elsewhere (47), layer 5 terminals from S1 and V1 overlap convincingly with HO thalamic cells that send projections to S1 and V1 (Figs. 4*A* and 5*A* and detailed in *SI Appendix*, Fig. S4 *A* and *E*), while layer 5 terminals from higher cortical areas appear to overlap only partially with these cells (Figs. 4 *B* and *C* and 5*B* and *SI Appendix*, Fig. S4 *B, C,* and *F*). However, our data show that these partially overlapping terminal fields from layer 5 of higher cortical areas also contribute driving input to some of the POm → S1 and Pul → V1 cells in adults, possibly via relatively few robust axons whose fluorescence signal is overwhelmed by nearby denser terminal fields. These synapses were not identified in a previous study of S1 and M1 connectivity through thalamus (47), likely due to small cortical injections allowing for topographical mismatch between S1 and M1. It is also the case that HO thalamic dendrites are not confined to well-defined input zones (36, 37). Therefore, while reciprocal loops undoubtedly contribute driving input to HO thalamus, the current results suggest that these reciprocal transthalamic feedback loops exist nested within "open" transthalamic pathways connecting separate cortical areas in both the feedforward and feedback directions.

**Subcortical Inputs to POm → S1 and Pul → V1.** Several subcortical sources of input to HO thalamus were also identified in our g-deleted-rabies experiments (e.g., SC is known to send input to both POm and Pul), and we have attempted to understand where those subcortical inputs fit into our model of HO thalamus. In our optogenetics assisted circuit mapping

experiment in the visual system, stimulating layer 5 cells from V1 or higher visual area LM evoked depressing EPSCs on retrolabeled Pul → V1 cells in both the striate-recipient (more rostral) Pul and SC-recipient (more caudal/lateral) Pul. These results are consistent with the idea that the rostral Pul → V1 population is cortically-driven without much subcortical input, much as in our findings on the POm → S1 pathway. On the other hand, the lateral Pul → V1 population can apparently still receive driving input from layer 5 of V1 and HVAs, but also receives dense subcortical innervation from SC. This view is also supported by the recent finding (26) that individual cells in lateral Pul can receive convergent driving input from layer 5 of V1 and SC.

In the somatosensory system, the sparsity of SpV input to the POm → S1 pathway was of particular interest to us. SpV densely innervates POm, and stimulation of SpV afferents evokes a mixture of driver and modulator-type responses in POm (35). However, our population-specific retrograde labeling failed to reveal a feedforward circuit from SpV to POm → S1 cells, and optogenetic SpV activation failed to evoke EPSCs onto retrolabeled POm → S1 cells. These data call into question the routing of the paralemniscal pathway through POm to S1, but agree with recent findings by El-Boustani et al. (25) that suggest that SpV input may preferentially innervate POm → S2 cells. It is not known whether the bottom-up inputs from SpV converge onto the same POm → S2 cells comprising the feedforward transthalamic pathway (S1 → POm → S2), or whether these are two separate populations of POm → S2 cells.

**Transthalamic Feedback Pathways Appear Modulatory While Feedforward Ones Appear to Drive Higher Cortical Areas.** Our data suggest that feedback through thalamus is generally modulatory while feedforward transthalamic pathways can strongly drive activity in higher cortical areas. A few implications of this hypothesis are noteworthy.

First, the marked homogeneity of responses in each cortical area reported here (e.g., all driver-type responses from POm to S2 and Pul to HVAs) suggest the possibility that feedback through thalamus could skip over cortical areas of intermediate hierarchical position and only modulate primary sensory cortex. That is, no modulator-type responses were observed in areas S2 or LM, even though both are considered to be hierarchically secondary and therefore might be expected to receive feedback from even higher-order cortical areas. It may be true that areas highest along the cortical hierarchy indirectly exert feedback control over intermediate areas through transthalamic feedback modulation of primary cortex. Alternatively, cortical hierarchy in the mouse may be "shallower" than in other species, such that no cortical area is in a position to send robust feedback signals to S2 or HVA LM. Or last, feedback to these areas through HO thalamus may violate our hypothesis and act as a driver.

Second, while transthalamic communication from layer 5 of S1 → POm → M1 had been described previously to drive M1 activity (11), our data verify the existence of a modulatory transthalamic pathway from layer 5 of M1 → POm → S1. Because POm projections to M1 appear to be driver to all layers (11) while POm projections to S1 are modulatory as described here, these two transthalamic pathways appear to have distinct functions. If the hypothesis is correct that feedforward routes through thalamus are drivers while feedback through thalamus is modulatory, this suggests a sensorimotor hierarchy in which S1 is lower than M1.

Last, these data also support the hypothesis that all direct corticocortical projections are paralleled by transthalamic pathways, now with our evidence that this pattern also exists in the feedback direction. It has been suggested that in corticocortical communication feedforward projections are more specifically organized and robust while feedback projections are more diffuse and likely to be modulatory (50). However, limited data have shown in the mouse that, in direct connections between V1 and HVAs as well as between A1 and A2, a mixture of driver and modulator inputs exist in both directions (41, 51), raising the possibility that purely feedforward driver and feedback modulator inputs are limited to transthalamic circuitry.

Given their organizational conservation across systems, it is likely that reciprocal and nonreciprocal connections between cortex and HO thalamus are critical to the stability of cortical representations and are integral to the flow of information in the brain. However, several key questions remain: Why do cortical areas that are directly connected to each other have additional transthalamic connections through HO thalamus in both feedforward and feedback directions? Does this parallel pattern always exist, or are some cortical areas connected by just direct or transthalamic pathways? How do transthalamic and corticocortical routes of information recombine in target areas? Is such integration different in the feedforward and feedback directions? Finally, how general is the pattern that feedforward transthalamic pathways operate in a driver capacity, and feedback, in a modulatory one?

## Materials and Methods

**Animals.** Experiments were approved by the Institutional Animal Care and Use Committee at the University of Chicago. Transgenic mice expressing cre recombinase in layer 5 of cortex were bred by crossing male Rbp4-cre KL100Gsat/Mmcd mice (GENSAT RP24-285K21) with female C57BL6J mice. Cre positive offspring of both sexes were used in experiments, along with wild type C57BL6J mice (JAX).

**Surgeries.** Stereotactic injections of viruses and tracers were performed as previously described (11) using a 0.5 $\mu$L Hamilton syringe. Surgeries for optogenetics were performed at p17-25 with coordinates in mm from bregma as follows (AP, ML, DV):

S1 : $-0.7$, $+3.1$, $-0.5$; M1 : $+1.1$, $+1.2$, $-0.5$; S2 : $-0.1$, $+4.0$, $-1.0$; V1 : $-4.2$, $+2.2$, $-0.5$; HVA $-$ LM : $-4.0$, $+3.5$, $-0.8$; POm : $-2.0$, $+1.25$, $-3.1$; Pul : $-1.8$, $+1.25$, $-2.4$ SpV : $-6.5$, $+1.9$, $-5.0$.

Surgeries for G-Deleted rabies tracing were performed at age 8 wk, with coordinates from bregma as follows:

S1 : $-0.8$, $+3.1$, $-0.5$; V1 : $-4.2$, $+2.2$, $-0.5$; POm : $-2.2$, $+1.25$, $-3.2$; Pul : $-1.9$, $+1.25$, $-2.5$

**Viruses and Tracers.** For optogenetics experiments, 50–90 nL of AAV9-pACAGW-ChR2-Venus (Addgene, 20071-AAV9) was injected to allow photostimulation and visualization of thalamocortical projections, 200 nL were injected for SpV, and 120–300 nL of AAV9-pAAV-EF1a-DIO-hChR2(H134R)-EYFP-WPRE-HGHpA (Addgene, 20298-AAV9) was used to allow photostimulation and visualization of layer 5 corticothalamic projections in a cre-dependent fashion, depending on the injection target. Three weeks were given for expression before recordings were obtained.

For retrograde labeling of thalamocortical projections to cortex, 150–300 nL of 10% Fluororuby (Thermo Fisher: D1817) in PBS was injected into appropriate cortical regions. Fluororuby is known to label cell bodies and sometimes processes without altering electrophysiological properties (11).

For G-deleted rabies tracing experiments, a protocol was developed using minimal viral volumes for sparse labeling, as described below. A total of 200 nL of either CAV2-CMV-Cre (Montpellier Vectorology, Institut de Génétique

Moléculaire de Montpellier) or AAVretro-Ef1a-Cre (Salk Institute, 55636) was injected in cortical areas S1 or V1 to deliver cre retrogradely to higher-order thalamus. At the same time, 80 nL of a 1:1 mixture of AAV8-CAG-FLEX-TCB (TVA-mCherry) and AAV8-CAG-FLEX-oG-WPRE-SV40-PA (Optimized G) (Salk Institute, 48332 and 74292, respectively) was injected into the relevant HO thalamic nucleus, POm, or Pul. After 3 wk allowing for expression, 80 nL EnvA-G-Deleted Rabies-eGFP (Salk Institute, 32635) was injected also in POm or Pul.

**Strategy for G-Deleted-RV Tracing.** For this output-defined G-deleted-rabies tracing strategy (31, 32), there is always a concern that a small percentage of cells in the "starter" region (here POm and Pul) may express TVA-mCherry and G in a cre-independent fashion without receiving cre from the relevant projection region, and thus retrogradely labeling spurious "input" cells merely projecting to the region. Likewise, there is a possibility for a small percentage of cre-expressing cells in the projection regions, S1 and V1, to pick up the cre-dependent TVA-mCherry and pseudotyped RV-GFP in thalamus, allowing for spurious GFP+ labeling in cortex. To avoid this second scenario, all cortical GFP+ input cells were screened for MCherry labeling (they should be GFP+ mCherry- unless incidental retrograde labeling from thalamus occurred). No mCherry labeling was observed outside of thalamus in the animals included in analysis. To minimize the probability of either pitfall affecting results, a protocol was designed to sparsely label the relevant "starters" and "inputs" with relatively small viral volumes. This approach allowed careful manual screening of each labeled cell through a 10× objective, and any data were discarded from animals with any spuriously double-labeled cells in cortex or starter cells in the neighboring FO thalamic nuclei outside of the target zone.

Images taken through a 5× objective were overlaid with the Allen Institute Mouse Brain Atlas for assessment of subcortical and cortical areas. Cortical layers were determined using these lines, distance from the pia (dorsal surface of cortex), and other visible landmarks (such as barrels in S1). Negative controls without Cre were also assessed and found to have small amounts of mCherry labeling in thalamus, but no cre-independent GFP labeling of inputs (*SI Appendix*, Figs. S2 and S3). While this approach limits the quantitative assessment of large numbers of labeled cells, such assessments can be affected by poorly understood cell-type biases. We find this sparse labeling approach yields more reliable qualitative data about synaptic inputs to heterogeneously organized brain areas such as HO thalamus.

**Anatomical Tissue Preparation and Microscopy.** As described previously (18), animals were transcardially perfused with phosphate-buffered saline followed by 4% paraformaldehyde in phosphate-buffered saline, pH 7.4. The brain was extracted and postfixed in 4% paraformaldehyde for at least 12 h before transferring to a cold 30% sucrose solution for >48 h. Brains were then cryosectioned coronally at 40-$\mu$m thick on a sliding microtome.

Brain sections were mounted on Superfrost Plus (Fisher Scientific) slides and coverslipped with DPX or Vectashield with DAPI (Vector Laboratories). A microscope with a 100 W mercury lamp with fluorescence optics (Leica Microsystems) was used to image the sections and photos were taken with a Retiga 2000 monochrome CCD camera and Q Capture Pro software (Qimaging). Leica TX2 filter cubes (excitation 560 nm, emission 645 nm, dichroic 595 nm) were used to visualize Fluoro-Ruby and mCherry fluorescence, L5 filter cubes (excitation 480 nm, emission 527 nm, dichroic 505 nm) were used to visualize GFP and eYPF fluorescence. Q Capture Pro software and FIJI (NIH) were used to overlay images and adjust brightness and contrast. High-resolution photomicrographs of input cells were captured with LAS AF Leica software on a Leica SP5 Tandem Scanner Spectral 2-phtoon confocal microscope.

**Electrophysiological Slice Preparation.** Animals were anesthetized to be nonresponsive to toe pinch and transcardially perfused with 4 mL of cold oxygenated (95% $O_2$, 5% $CO_2$) artificial cerebrospinal fluid, which contained the following (in mM): 125 NaCl, 25 NaHCO$_3$, 3 KCl, 1.25 NaH$_2$PO$_4$, 1 MgCl$_2$, 2 CaCl$_2$, and 25 glucose. The brain was extracted, blocked in accordance with the desired slice angle (see below), glue-mounted on a vibratome platform (Leica), and sliced in cold (1–4 °C), oxygenated slicing solution containing the following (in mm): 2.5 KCl, 1.25 NaH$_2$PO$_4$, 10 MgSO$_4$, 0.5 CaCl$_2$, 25 NaHCO$_3$, 11 glucose, and 206 sucrose. Slices were cut at 420-$\mu$m thickness.

While many recordings could be made in coronal slices, to facilitate the distant optical stimulation of presynaptic axons, for recordings in cortex, many

brains were cut at angles preserving some but not all of the complete circuit, referred to as "pseudo-connected" slices. For somatosensory thalamocortical projections, brains were cut at 55° from the midline and 10° from the horizontal to preserve thalamocortical projections (27). For visual thalamocortical projections, brains were cut at 55° from horizontal as in MacLean et al. (28). In experiments recording in thalamus, slices were made coronally.

Brain slices were then transferred to 33 °C oxygenated artificial cerebrospinal fluid that was allowed to return to room temperature thereafter. Recovery in artificial cerebrospinal fluid occurred in the dark for at least 1 h and all slicing and patching were performed in minimal light.

**Whole-Cell Recordings.** Slices containing the relevant regions of thalamus or cortex were visualized using differential interference contrast with a Axioskop 2FS microscope (Carl Zeiss). Fluorescent ChR2 expression was confirmed using the 5× air objective with a fluorescein isothiocyanate filter (set 37; Zeiss) and Fluororuby-labeled cells were identified under 40× magnification with a rhodamine filter (set 15; Zeiss). Recordings were made with a Multiclamp 700B amplifier and pCLAMP software (Molecular Devices). Recording glass pipettes with 4–6 MΩ resistance were filled with intracellular solution containing the following (in mm): 117 K-gluconate, 13 KCl, 1 $MgCl_2$, 0.07 $CaCl_2$, 10 Hepes, 0.1 EGTA, 2 $Na_2$-ATP, 0.4 Na-GTP, pH 7.3, 290 mOsm, and 0.5–1 dinitrostilbene-2,2-disulfonic acid (a $GABA_A$ antagonist). Pharmacological inactivation of iGluRs was induced by bath application of 50 μM DNQX and 100 μM AP5, while group I mGluRs were blocked with 40 μM LY367385 and 30 μM MPEP. The locations of each patched cell within cortex was imaged along with its recording pipette and assigned to a layer by distance from pia and white matter, along with differences in transmitted brightness under DIC, and relation to other relevant landmarks (e.g., barrels in S1). Transition areas near laminar borders were avoided. Once whole-cell recordings were achieved, the excitatory identity of thalamic relay cells were verified by characteristic responses to current injections (rebound bursts in response to hyperpolarization). The excitatory identity of cells in cortex was verified by layer and area-specific responses to positive and negative current injections which easily distinguish GABAergic interneurons (52), as well as by size and shape (all excitatory cells were pyramidal with the exception of S1 layer 4), as described previously (22, 23, 52).

Optogenetic stimulation was delivered using a 355 nm laser (DPSS: 3505–100), controlled with galvanometer mirrors (Cambridge Technology) focused on the slice through a 5× air objective using custom software in MATLAB (MathWorks). Four pulses of 1-ms duration were delivered at 100 ms interstimulus interval (ISI) during recordings in voltage clamp. Laser intensity at the

slice was varied by a neutral density filter wheel before in the beam path. Stimulations were attempted at low intensity before slowly increasing until postsynaptic responses were observed. At a typically used intensity for near-threshold activation, the beam produced an 80-μm diameter illuminated spot with a power of 5 mW at the level of the slice using an optical power meter (Thorlabs). Focal laser stimulation was directed either over the patched cell to activate the ChR2-expressing presynaptic terminals or at a distance of >300 μm away to activate distant ChR2-expressing axons in accordance with previous work (18). For high-frequency optogenetic stimulation, 20 pulses of 1-ms duration were delivered at 12 ms ISI (83 Hz), and responses were recorded in current clamp. Electrical stimulation of POm → S1 pathway was achieved with a 2 × 1 matrix tungsten bipolar electrode with 115-μm separation (FHC) placed along labeled thalamocortical fibers in the internal capsule. Four 0.1-ms-long pulses were delivered at 10 Hz.

**Data Analysis and Statistics.** Electrophysiological data were collected using custom MATLAB software and analyzed using RStudio (v1.3.959). The amplitude of responses to stimulation pulses was measured by subtracting the average value for 20 ms before the delivery of a pulse (baseline) from the maximum value of the peak. The PPR was calculated by dividing the amplitude of the second pulse by that of the first pulse. Statistical analyses were also conducted in RStudio. All comparisons between groups are Mann-Whitney U tests, except for the comparison of the driver/modulator ratio observed in our recordings in S2 and HVAs with the driver/modulator ratio from FO thalamic stimulations recorded in S1 and A1 from Viaene et al. (23), which used a $\chi^2$ test with Yates correction. Image analysis was conducted in FIJI (NIH), and figures were produced using Corel Draw (v21).

**Data Availability.** All study data are included in the article and/or *SI Appendix*.

Author affiliations: ᵃDepartment of Neurobiology, University of Chicago, Chicago, IL 60637

1. S. M. Sherman, Thalamus plays a central role in ongoing cortical functioning. *Nat. Neurosci.* **19**, 533–541 (2016).
2. M. Nakajima, M. M. Halassa, Thalamic control of functional cortical connectivity. *Curr. Opin. Neurobiol.* **44**, 127–131 (2017).
3. Y. B. Saalmann, S. Kastner, The cognitive thalamus. *Front. Syst. Neurosci.* **9**, 39 (2015).
4. S. M. Sherman, R. W. Guillery, *Functional Connections of Cortical Areas: A New View from the Thalamus* (MIT Press, 2013).
5. S. M. Sherman, W. M. Usrey, *Exploring Thalamocortical Interactions: Circuitry for Sensation, Action, and Cognition* (Oxford University Press, 2021).
6. W. Zhang, R. M. Bruno, High-order thalamic inputs to primary somatosensory cortex are stronger and longer lasting than cortical inputs. *eLife* **8**, e44158 (2019).
7. R. A. Mease, M. Metz, A. Groh, Cortical sensory responses are enhanced by the higher-order thalamus. *Cell Rep.* **14**, 208–215 (2016).
8. A. Groh *et al.*, Convergence of cortical and sensory driver inputs on single thalamocortical cells. *Cereb. Cortex* **24**, 3167–3179 (2014).
9. B. M. Hooks, Sensorimotor convergence in circuitry of the motor cortex. *Neuroscientist* **23**, 251–263 (2017).
10. N. Urbain *et al.*, Whisking-related changes in neuronal firing and membrane potential dynamics in the somatosensory cortex of awake mice. *Cell Rep.* **13**, 647–656 (2015).
11. C. Mo, S. M. Sherman, A sensorimotor pathway via higher-order thalamus. *J. Neurosci.* **39**, 692–704 (2019).
12. B. B. Theyel, D. A. Llano, S. M. Sherman, The corticothalamocortical circuit drives higher-order cortex in the mouse. *Nat. Neurosci.* **13**, 84–88 (2010).
13. V. Sampathkumar, A. Miller-Hansen, S. M. Sherman, N. Kasthuri, Integration of signals from different cortical areas in higher order thalamic neurons. *Proc. Natl. Acad. Sci. U.S.A.* **118**, e2104137118 (2021).
14. R. D. Rafal, M. I. Posner, Deficits in human visual spatial attention following thalamic lesions. *Proc. Natl. Acad. Sci. U.S.A.* **84**, 7349–7353 (1987).
15. R. Ward, S. Danziger, V. Owen, R. Rafal, Deficits in spatial coding and feature binding following damage to spatiotopic maps in the human pulvinar. *Nat. Neurosci.* **5**, 99–100 (2002).
16. J. C. Snow, H. A. Allen, R. D. Rafal, G. W. Humphreys, Impaired attentional selection following lesions to human pulvinar: Evidence for homology between human and monkey. *Proc. Natl. Acad. Sci. U.S.A.* **106**, 4054–4059 (2009).
17. B. O. F. de Souza, N. Cortes, C. Casanova, Pulvinar modulates contrast responses in the visual cortex as a function of cortical hierarchy. *Cereb. Cortex* **30**, 1068–1086 (2020).
18. G. Purushothaman, R. Marion, K. Li, V. A. Casagrande, Gating and control of primary visual cortex by pulvinar. *Nat. Neurosci.* **15**, 905–912 (2012).
19. M. M. Roth *et al.*, Thalamic nuclei convey diverse contextual information to layer 1 of visual cortex. *Nat. Neurosci.* **19**, 299–307 (2016).
20. Y. B. Saalmann, M. A. Pinsk, L. Wang, X. Li, S. Kastner, The pulvinar regulates information transmission between cortical areas based on attention demands. *Science* **337**, 753–756 (2012).
21. M. E. Bickford, Thalamic circuit diversity: Modulation of the driver/modulator framework. *Front. Neural Circuits* **9**, 86 (2016).
22. A. N. Viaene, I. Petrof, S. M. Sherman, Properties of the thalamic projection from the posterior medial nucleus to primary and secondary somatosensory cortices in the mouse. *Proc. Natl. Acad. Sci. U.S.A.* **108**, 18156–18161 (2011).
23. A. N. Viaene, I. Petrof, S. M. Sherman, Synaptic properties of thalamic input to layers 2/3 and 4 of primary somatosensory and auditory cortices. *J. Neurophysiol.* **105**, 279–292 (2011).
24. A. Blot *et al.*, Visual intracortical and transthalamic pathways carry distinct information to cortical areas. *Neuron* **109**, 1996–2008.e6 (2021).
25. S. El-Boustani *et al.*, Anatomically and functionally distinct thalamocortical inputs to primary and secondary mouse whisker somatosensory cortices. *Nat. Commun.* **11**, 3342 (2020).
26. M. A. Kirchgessner, A. D. Franklin, E. M. Callaway, Distinct "driving" versus "modulatory" influences of different visual corticothalamic pathways. *Curr. Biol.* **31**, 5121–5137.e7 (2021).
27. A. Agmon, B. W. Connors, Thalamocortical responses of mouse somatosensory (barrel) cortex in vitro. *Neuroscience* **41**, 365–379 (1991).
28. J. N. MacLean, V. Fenstermaker, B. O. Watson, R. Yuste, A visual thalamocortical slice. *Nat. Methods* **3**, 129–134 (2006).
29. S. L. Jackman, B. M. Beneduce, I. R. Drew, W. G. Regehr, Achieving high-frequency optical control of synaptic transmission. *J. Neurosci.* **34**, 7704–7714 (2014).
30. A. N. Viaene, I. Petrof, S. M. Sherman, Activation requirements for metabotropic glutamate receptors. *Neurosci. Lett.* **541**, 67–72 (2013).
31. L. A. Schwarz *et al.*, Viral-genetic tracing of the input-output organization of a central noradrenaline circuit. *Nature* **524**, 88–92 (2015).
32. E. M. Callaway, L. Luo, Monosynaptic circuit tracing with glycoprotein-deleted rabies viruses. *J. Neurosci.* **35**, 8979–8985 (2015).

33. I. Reichova, S. M. Sherman, Somatosensory corticothalamic projections: Distinguishing drivers from modulators. *J. Neurophysiol.* **92**, 2185–2197 (2004).

34. P. Veinante, M. F. Jacquin, M. Deschênes, Thalamic projections from the whisker-sensitive regions of the spinal trigeminal complex in the rat. *J. Comp. Neurol.* **420**, 233–243 (2000).

35. C. Mo, I. Petrof, A. N. Viaene, S. M. Sherman, Synaptic properties of the lemniscal and paralemniscal pathways to the mouse somatosensory thalamus. *Proc. Natl. Acad. Sci. U.S.A.* **114**, E6212–E6221 (2017).

36. H. Nakamura, H. Hioki, T. Furuta, T. Kaneko, Different cortical projections from three subdivisions of the rat lateral posterior thalamic nucleus: A single-neuron tracing study with viral vectors. *Eur. J. Neurosci.* **41**, 1294–1310 (2015).

37. N. A. Zhou, P. S. Maire, S. P. Masterson, M. E. Bickford, The mouse pulvinar nucleus: Organization of the tectorecipient zones. *Vis. Neurosci.* **34**, E011 (2017).

38. A. M. Thomson, Facilitation, augmentation and potentiation at central synapses. *Trends Neurosci.* **23**, 305–312 (2000).

39. S. M. Sherman, R. W. Guillery, On the actions that one nerve cell can have on another: Distinguishing "drivers" from "modulators". *Proc. Natl. Acad. Sci. U.S.A.* **95**, 7121–7126 (1998).

40. M. E. Diamond, M. Armstrong-James, F. F. Ebner, Somatic sensory responses in the rostral sector of the posterior group (POm) and in the ventral posterior medial nucleus (VPM) of the rat thalamus. *J. Comp. Neurol.* **318**, 462–476 (1992).

41. E. N. Covic, S. M. Sherman, Synaptic properties of connections between the primary and secondary auditory cortices in mice. *Cereb. Cortex* **21**, 2425–2441 (2011).

42. I. Petrof, A. N. Viaene, S. M. Sherman, Properties of the primary somatosensory cortex projection to the primary motor cortex in the mouse. *J. Neurophysiol.* **113**, 2400–2407 (2015).

43. V. Sampathkumar, A. Miller-Hansen, S. Murray Sherman, N. Kasthuri, An ultrastructural connectomic analysis of a higher-order thalamocortical circuit in the mouse. *Eur. J. Neurosci.* **53**, 750–762 (2021).

44. Q. Wang, E. Gao, A. Burkhalter, Gateways of ventral and dorsal streams in mouse visual cortex. *J. Neurosci.* **31**, 1905–1918 (2011).

45. J. H. Siegle *et al.*, Survey of spiking in the mouse visual system reveals functional hierarchy. *Nature* **592**, 86–92 (2021).

46. Q. Fang *et al.*, A differential circuit via retino-colliculo-pulvinar pathway enhances feature selectivity in visual cortex through surround suppression. *Neuron* **105**, 355–369.e6 (2020).

47. K. Guo, N. Yamawaki, J. M. Barrett, M. Tapies, G. M. G. Shepherd, Cortico-thalamo-cortical circuits of mouse forelimb S1 are organized primarily as recurrent loops. *J. Neurosci.* **40**, 2849–2858 (2020).

48. A. L. Juavinett, E. J. Kim, H. C. Collins, E. M. Callaway, A systematic topographical relationship between mouse lateral posterior thalamic neurons and their visual cortical projection targets. *J. Comp. Neurol.* **528**, 95–107 (2020).

49. F. Crick, C. Koch, Constraints on cortical and thalamic projections: The no-strong-loops hypothesis. *Nature* **391**, 245–250 (1998).

50. E. M. Callaway, Feedforward, feedback and inhibitory connections in primate visual cortex. *Neural Netw.* **17**, 625–632 (2004).

51. R. De Pasquale, S. M. Sherman, Synaptic properties of corticocortical connections between the primary and secondary visual cortical areas in the mouse. *J. Neurosci.* **31**, 16494–16506 (2011).

52. F. Scala *et al.*, Layer 4 of mouse neocortex differs in cell types and circuit organization between sensory areas. *Nat. Commun.* **10**, 4174 (2019).